

# Formation of Hybrid Membranes for Water Desalination by Membrane Distillation

I. I. Vinogradov<sup>a</sup>, N. A. Drozhzhin<sup>a</sup>, L. I. Kravets<sup>a, \*</sup>, A. Rossouw<sup>a</sup>, T. N. Vershinina<sup>a</sup>, and A. N. Nechaev<sup>a, b</sup>

<sup>a</sup> Joint Institute of Nuclear Research, Dubna, Moscow oblast, 141980 Russia

<sup>b</sup> Dubna State University, Dubna, Moscow oblast, 141980 Russia

\*e-mail: [kravets@jinr.ru](mailto:kravets@jinr.ru)

Received May 29, 2024; revised July 12, 2024; accepted July 14, 2024

**Abstract**—A method has been developed for the formation of hybrid membranes consisting of a hydrophilic microporous substrate and a hydrophobic nanofibrous polymer layer deposited by electrospinning. A track-etched poly(ethylene terephthalate) membrane has been used as the hydrophilic microporous substrate, onto the surface of which a thin layer of titanium is deposited by magnetron sputtering to provide the nanofibrous layer with adhesion. Simultaneously, this layer has been used as an electrode of a deposition collector for the electrospinning formation of the nanofibrous coating. It has been shown that the application of this method for the preparation of polymer coatings using poly(vinylidene fluoride) as a starting material for the formation of nanofibers makes it possible to obtain a highly hydrophobic layer, the surface of which has an average water contact angle of  $143.3 \pm 1.3^\circ$  depending on the deposition density. The morphological study of the nanofibrous coating has shown that its microstructure is typical of nonwoven materials. The nanofibers that form the porous system of this layer have a wide scatter of sizes. FTIR spectroscopic and X-ray diffraction investigations of the molecular structure of the nanofibrous layer have shown that the  $\beta$ -phase prevails in its structure, with this phase being characterized by the maximum dipole moment. It has been shown that the elaborated hybrid membranes ensure high separation selectivity of desalinating an aqueous 26.5 g/L sodium chloride solution by the membrane distillation method. In the studied regime of the membrane distillation, the salt rejection coefficient for membranes with nanofibrous layer densities of  $20.7 \pm 0.2$ – $27.6 \pm 0.2$  g/m<sup>2</sup> is 99.97–99.98%. It has been found that the use of a highly hydrophobic nanofibrous layer with a developed porous structure in combination with a hydrophilic microporous substrate makes it possible to increase the productivity of the membrane distillation process. The value of the maximum condensate flow through the membranes is, on average, 7.0 kg m<sup>2</sup>/h, and its value depends on the density of the deposited nanofibrous layer.

**Keywords:** hydrophilic track-etched membrane, electrospinning of nanofibers, poly(vinylidene fluoride), highly hydrophobic layer, hybrid membranes, water desalination

**DOI:** 10.1134/S1061933X24600519

## INTRODUCTION

In the new millennium, the production of drinking water is becoming a global problem for humanity. The growing shortage of fresh water can be compensated by desalination of seawater. Various methods can be used for this purpose, such as distillation, reverse osmosis, electrodialysis, ion exchange, etc. [1]. Membrane distillation (MD) is, at present, one of the promising methods for water desalination. This method is based on the permeability of a microporous membrane to water vapor and its impermeability to liquid water [2–6]. It has a number of advantages over other processes, with the main one being the high separation selectivity. Operating temperatures of membrane distillation are much lower (commonly, the temperature of a mixture being separated is in a range of 50–80°C) than that of the traditional distillation process. Therefore, there is no need to heat the mixture to the boiling

point in this case. This makes this process to be economically attractive. Since the driving force of MD is the difference in temperatures rather than pressures, the operating pressures are low compared to membrane processes such as reverse osmosis. This makes the MD process to be technologically safer. In addition, when MD is implemented, heat losses to the environment are insignificant as compared with other processes.

Various membrane distillation modules (MDMs) are used to carry out the MD process. Currently, four main configurations of the modules are used to realize this process: a direct contact membrane distiller, an air gap membrane distiller, a sweeping gas membrane distiller, and a vacuum membrane distiller [2, 3]. The configuration of the air gap module is optimum, because the air gap provides a significant reduction in the heat losses as compared with other modules owing to the presence of a condensing partition and a greater

temperature difference between the hot and cooled surfaces, and also it provides a higher thermal energy for water evaporation [5, 6].

Membranes are the basic elements of the separating modules used in the MD processes. Commercial hydrophobic microfiltration membranes produced from polypropylene (PP), poly(vinylidene fluoride) (PVDF), and polytetrafluoroethylene (PTFE) are commonly used for these purposes. Their key property is the low wettability of their surfaces, which prevents water from penetrating into vapor-filled pores. Due to their considerable thickness, these membranes have a high resistance to mass transfer and, hence, a low productivity. To successfully implement the processes of salt water desalination, it is necessary to create a new generation of highly productive membranes that would be efficient in thermogradient (occurring under the action of temperature gradients) separation processes, which include the MD method.

An efficient approach to creating membranes for MD is the functionalization of hydrophilic membrane surfaces, as the essence of which is imparting new functional properties to membranes by a partial or complete change in the composition of the chemical groups in surface layers, as well as by a modification of the surface morphology [7–9]. One of the methods for functionalizing membranes is the deposition of diverse thin polymer coatings onto their surfaces [10–14]. Such a modification leads to the formation of composite membranes (CMs) that consist of a porous substrate, i.e., the original membrane, and a deposited polymer layer. The deposition of a polymer coating makes it possible to finely tune the chemical and physical properties of resulting composite membranes to improve their service characteristics, including surface wettability. Of greatest interest for the production of membranes specifically designed for MD is the development of methods for creating bilayer composite membranes, in which one of the layers is a hydrophilic support, while the other thin layer, which determines the functional properties of the created membranes, has hydrophobic properties. The combination of a thin hydrophobic layer with a thick hydrophilic support makes it possible to increase the permeate flow through a membrane.

A number of modern modification methods can be used to apply hydrophobic polymer coatings onto membrane surfaces. Of greatest interest are methods for forming coatings from an active gaseous phase [15]. This group of the methods includes the deposition of coatings due to polymerization of low-molecular-weight organic compounds resulting from the dispersion of polymers under the action of laser radiation [16, 17], radio-frequency discharge plasma [18, 19], or a beam of accelerated electrons [20–23]. This approach is distinguished by the simultaneous occurrence of two main stages, namely, the stage of forming volatile low-molecular-weight products and the stage

of their activation, which is understood as the process of transition to a reactive state. These methods are high-tech and make it possible to regulate the structure and composition of deposited layers, as well as to produce highly hydrophobic and superhydrophobic coatings on solid surfaces [21–23].

For example, it was shown in [23] that the deposition of coatings from an active gaseous phase obtained by electron-beam dispersion of PTFE onto the surface of a track-etched membrane (TM) made of poly(ethylene terephthalate) (PET) led to significant hydrophobization of the membrane surface layer, with the hydrophobization degree being dependent on the coating thickness. When a polymer layer 100 nm thick was deposited, a coating was formed that had highly hydrophobic properties and a water contact angle of 130°. An increase in the thickness of the deposited layer to 500 nm due to a significant growth of the surface roughness led to the formation of a coating with superhydrophobic properties and a contact angle of 155°. The resulting composite membranes, as compared with the original membrane, showed higher separation selectivity when desalinating an aqueous sodium chloride solution by the membrane distillation method. In addition, the productivity of bilayer composite membranes in the MD process was higher than that of the original track-etched PP membrane due to the low resistance to the mass transfer (owing to a reduction in the path length of water vapor transfer through the hydrophobic PTFE coating layer). The distillate resulting from the MD process satisfied the requirements imposed on drinking water and process water used in many technologies.

Therewith, electrospun nanofibrous membranes are, at present, widely used in MD processes for water desalination along with thin-layer composite membranes [24–29]. The production of such membranes consists in applying a static electric field to a jet of a polymer solution or melt escaping from a small die. As a result, the polymer jet is charged and dispersed into jets of smaller (down to the nanometer range) diameters due to electrostatic repulsion. During the flight stage, the jet dries up, and the resulting nanofibers are accumulated on the surface of a collector to form a flat sheet [30, 31]. Compared to commercial hydrophobic microfiltration membranes, nanofibrous membranes made of PVDF and PTFE have a higher degree of hydrophobicity due to their developed porous structure. In addition, they exhibit a greater productivity in the MD processes of water desalination due to their high bulk porosity. The listed advantages are compensated by the insufficient mechanical strength of such membranes and, as a result, the need to use membranes of considerable thicknesses, as well as the difficulty of obtaining a repeating (identical) pore structure.

In this regard, a promising way to creating polymer membranes for MD aimed at water desalination may, in our opinion, be the method proposed in [32–34] for

the formation of hybrid membranes by depositing a nanofibrous polymer layer of chitosan onto the surface of a TM using the electrospinning method. The adhesion of the nanofibrous layer to the TM surface was provided by using a thin layer of pre-sputtered titanium, which simultaneously served as the electrode of the deposition collector during the electrospinning process [35]. The increased adhesion of the nanofibrous chitosan layer to the titanium surface can be explained by the covalent binding of the film of titanium oxides covering the metal (the presence of this film was shown in [35]) with the surface functional groups of chitosan [36]. It may be assumed that the use of a combination of a hydrophilic track-etched membrane and a hydrophobic nanofibrous polymer layer having different pore geometries will make it possible to obtain an optimum membrane structure with a set of properties required for the MD process. The use of a track-etched membrane as a porous substrate having strictly calibrated cylindrical pores will make it possible not only to control the permeability of water vapor but also to improve the mechanical properties of the hybrid membrane as a whole. The hydrophobic nanofibrous layer with a high porosity will significantly increase the productivity of the membranes of this type.

Thus, the goal of this work was creating and studying the properties of a hybrid membrane that could be used in the MD processes for water desalination. As a hydrophilic porous substrate, we used a bilayer composite membrane consisting of a poly(ethylene terephthalate) track-etched membrane with a thin titanium layer applied onto its surface. Poly(vinylidene fluoride) was used to form a hydrophobic nanofibrous layer. The efficiency of the developed membranes was assessed using the process of aqueous sodium chloride solution desalination by the air gap MD method.

## EXPERIMENTAL

In the experiments, we used a PET TM with an effective pore diameter of 0.3  $\mu\text{m}$  obtained on the basis of the Hostaphan RNK polymer film produced by Mitsubishi polyester film Co. (Germany) with a nominal thickness of 23.0  $\mu\text{m}$ . The membrane was obtained by irradiating the initial film with positively charged krypton ions having an energy of  $\sim 3$  MeV/nucleon accelerated in a U-400 cyclotron. The ion fluence was  $(2.7 \pm 0.3) \times 10^8$   $\text{cm}^{-2}$ . In order to form pores, the irradiated film was chemically etched at a temperature of 75°C in an aqueous 3 mol/L sodium hydroxide solution according to the procedure described in [37]. Before etching, the selectivity of the track etching process was increased by subjecting the film to UV radiation having a maximum intensity at 310–320 nm. When studying the membrane distillation process for water desalination, a commercial hydrophobic PVDF membrane (Durapore, Merck) with a pore size of 0.45  $\mu\text{m}$  manufactured by the phase inversion method [38] was used as a reference sample.

Below, the membrane of this type is referred to as PVDF, Merck.

Titanium was sputtered onto the membrane surface using a UMN-180 extended magnetron sputterer equipped with a planar cathode (LLC Ivtekhnomash) according to the procedure described in detail in [35]. The coating was deposited by sputtering titanium with a purity of 99.7% from a vertically installed target in argon (99.99%). The thickness of the deposited layer was  $40 \pm 4$  nm. The membrane with the deposited titanium layer is denoted as TM (Ti).

To obtain a nanofibrous coating on the surface of the TM (Ti) membrane, an 8% spinning solution was prepared using PVDF with an average molecular weight of  $6 \times 10^5$  g/mol (BLD Pharm, China). A 60 : 40 (vol/vol) mixture of *N,N*-dimethylformamide (DMF, 99.8%, Sigma-Aldrich, Germany) and acetone (99.9%, PanReac AppliChem, Spain) was used as a solvent.

A nanofibrous PVDF layer was deposited onto the surface of the TM (Ti) membrane by electrospinning with the use of a Nanon-01A setup (MECC Co. LDT, Japan). An F90XSH200 mm drum collector with sizes of 29.7  $\times$  21 cm was chosen as a cathode. The following deposition regime was used: voltage, 25 kV; solution dosing rate, 1.4 mL/h; die size, 0.7 mm; distance between the die and the cathode, 15 cm; the angle between the die and the cathode, 90°; drum collector rotation rate, 50 rpm; velocity of die movement along the *X* axis, 1 cm/s; and spinning solution volumes, 5, 10, 15, and 20 mL. The densities of the nanofibrous layers deposited onto the surface of the TM (Ti) membrane were  $\sim 6.9 \pm 0.2$ ,  $13.8 \pm 0.2$ ,  $20.7 \pm 0.2$ , and  $27.6 \pm 0.2$  g/m<sup>2</sup>, respectively. Below, the series of the hybrid membrane samples obtained in this way is referred to as TM (Ti) + PVDF (V), where *V* is the volume of the spinning solution used for the electrospinning of nanofibers.

The following methods were employed to study the structure and properties of the hybrid membranes. The gas permeability of the membranes was determined with a POROLUX 1000 capillary flow porosimeter (POROMETER) using samples with a diameter of 25 mm. The operating gas pressure was 10<sup>4</sup> Pa.

The microstructure and morphology of membrane samples were studied using a “HITACHI” S-3400N high-resolution scanning electron microscope (SEM) (Japan) operating in the thermal emission and the secondary electron mode. The accelerating voltage was 15 kV. The obtained micrographs were processed in the Gatan Digital Micrograph software shell.

The wettabilities of the membrane surfaces were characterized by the values of the static water contact angles measured at room temperature by the sessile droplet method [39] using an “Easy Drop DSA100” setup (KRUSS, Germany) and the Drop Shape Analysis V.4 software. For this purpose, a 3- $\mu\text{L}$  water droplet was applied with a microsyringe onto the surface of

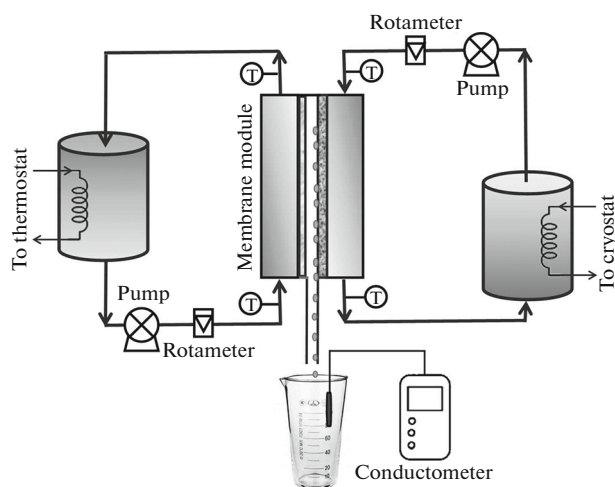


**Fig. 1.** Layout of the laboratory setup used to carry out the membrane distillation process.

a membrane. The image of the droplet was recorded with a video camera and digitized after reaching an equilibrium state, in which the droplet ceased to spread. The contact angle was determined as the angle between the surface of a wetted membrane and the line tangent to the curved surface of the droplet at the point of the three-phase contact. Deionized water with a specific resistance of 18.2 MΩ cm obtained using a Milli-Q Advantage A10 setup (Millipore, United States) was used for the measurements. The average values were obtained from at least five measurements for each membrane sample.

The values of  $LEP_w$  (water pressure at a membrane inlet) were determined according to the method described in [40]. A Millipore filtration cell was used for the measurements, which were performed for membrane samples with an effective area of 17.34 cm<sup>2</sup>. The cell was filled with deionized water; then, pressure was gradually applied to it from a balloon with air at a temperature of 23°C. The minimum pressure (equal to the value of  $LEP_w$ ), at which water penetrated into the interfiber space, was recorded. The  $LEP_w$  value was found by averaging at least three measurement results obtained for each membrane sample.

The surface functional groups were analyzed using a Nicolet iS20 FTIR spectrometer (Thermo Fisher Scientific) equipped with a Smart iTX attachment. All measurements were performed at a resolution of 4.0 cm<sup>-1</sup> and the number of scans equal to, at least, 32. The recorded spectra were processed in the Origin 2017 software shell. The absorption bands were assigned according to [41].

The X-ray diffraction (XRD) analysis was carried out with a PANalytical EMPYREAN powder diffractometer using CuK<sub>α</sub> radiation with a wavelength of 1.5406 Å. Diffraction patterns were obtained within an angle range of  $2\theta = 5^\circ - 60^\circ$  with steps of 0.026°. The

phase composition was determined using the PDF-4 database.

The applicability of the membranes to the desalination of an aqueous sodium chloride solution was experimentally studied with a laboratory setup (Fig. 1), which contained a vertically installed air gap MDM. The MDM was made of Kaprolon material (TC (technical certificate) 2224-036-00203803-2012, Russia). The working area of the membrane was  $5 \times 10^{-3}$  m<sup>2</sup>. The MDM consisted of two chambers separated by a membrane and a monolithic cooled partition. The thickness of the air gap between the membrane and the cooled partition was 4 mm. A hot flow (water being desalinated) passed through one of the chambers, and a flow of cold water moved through the other. The hot flow circulated in a closed loop between the MDM and a LOIP LT-100 water thermostat (Russia), which maintained a temperature of 65°C. The cold flow circulated in a closed circuit between the MDM and a LOIP FT-211-25 liquid cryostat (Russia), which maintained a temperature of 15°C. The temperatures of the solution being desalinated and water used to cool the monolithic partition were selected based on the analysis of the literature data, which are most completely presented in reviews [2–6]. The temperatures of the hot and cold flows at the inlet and outlet of the MDM were controlled with electronic thermometers having a division value of 0.1°C. Water being desalinated, the concentration of sodium chloride in which was 26.5 g/L, and cold water were thermostated in special containers according to the “water bath” principle. The movement of the hot and cold flows was initiated by LOIP LS-301 pumps (Russia). The flow rates in the hot solution and cold water chambers were equal to  $600 \pm 5$  mL/min. The rates of these flows were controlled by rotameters. The condensate being formed on the surface of the cooled partition flowed by gravity through a bottom fitting into a glass measuring cylinder. The volume of the condensate produced over a certain time was measured. The efficiency of the membrane distillation process was assessed using the salt rejection coefficient, which was calculated as the following ratio:

$$R(\%) = \frac{C_0 - C_x}{C_0} \times 100\%, \quad (1)$$

where  $C_0$  is the sodium chloride concentration in the initial solution and  $C_x$  is the sodium chloride concentration in the condensate. The salt concentrations in the initial solution and condensate were determined conductometrically using a Starter 3100C instrument (OHAUS Co., China). The measurement error was  $\pm 0.5\%$ . To maintain a constant concentration of sodium chloride during the experiments, deionized water was added to the container with the solution being desalinated every 30 min. The amount of added water corresponded to the measured volume of the condensate.

**Table 1.** Characteristics of the studied membrane samples

Membrane sample	Density of nanofibrous layer, g/m <sup>2</sup>	Air flow at $\Delta P = 10^4$ Pa, L/h cm <sup>2</sup>	Contact angle, deg	LEP <sub>w</sub> , kPa
TM (Ti)	—	41.6 ± 0.3	39.9 ± 3.5	—
PVDF, Merck	—	43.9 ± 0.2	124.3 ± 0.5	120 ± 2
TM (Ti) + PVDF (5)	6.9 ± 0.2	41.2 ± 0.2	144.3 ± 1.2	25 ± 1
TM (Ti) + PVDF (10)	13.8 ± 0.2	40.6 ± 0.2	140.9 ± 1.3	27 ± 1
TM (Ti) + PVDF (15)	20.7 ± 0.2	33.0 ± 0.3	143.2 ± 1.4	27 ± 1
TM (Ti) + PVDF (20)	27.6 ± 0.2	32.0 ± 0.4	144.7 ± 1.2	27 ± 1

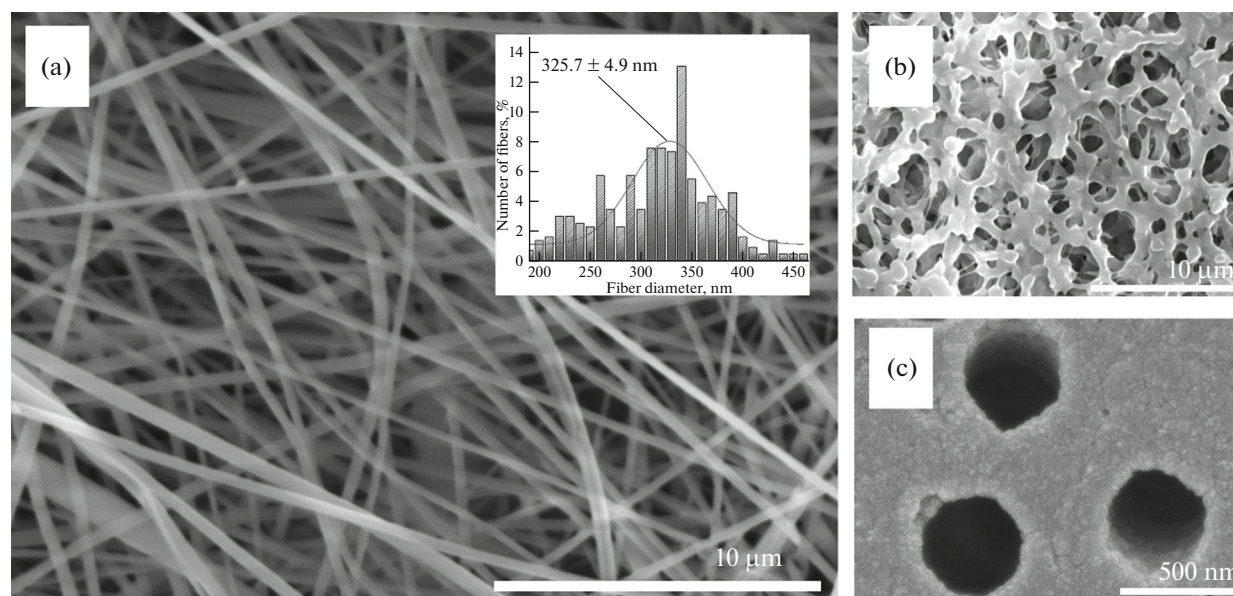
## RESULTS AND DISCUSSION

The results of measuring the characteristics of the TM (Ti) membrane, a commercial PVDF membrane (Durapore, Merck), and TM (Ti) + PVDF (V) hybrid membranes with different densities of the nanofibrous PVDF layer deposited by electrospinning are given in Table 1. As follows from the presented data, the deposition of the nanofibrous layer causes a slight decrease in the specific productivity with respect to air relative to the TM (Ti) membrane due to the partial closure of the pores on its surface. The formation of the nanofibrous PVDF layer on the surface of the TM (Ti) membrane is illustrated in Fig. 2a, which shows a SEM micrograph of the surface layer of the TM (Ti) + PVDF (10) membrane. It can be seen that the deposited layer consists of randomly arranged nanofibers, i.e., it has a random microstructure typical of nonwoven materials. The nanofiber diameter distribution histogram plotted on the basis of the analysis of the microphotograph is

shown in the inset of Fig. 2a. The average nanofiber diameter obtained by the Gaussian approximation of the data appeared to be  $325.7 \pm 4.9$  nm. Samples of the membranes with different densities of the deposited nanofibrous layer had almost the same microstructure; therefore, the micrographs of other samples are not presented.

Figure 2 also shows micrographs taken from the surface of the commercial PVDF membrane (Durapore, Merck), which was used to compare the results of desalinating the aqueous sodium chloride solution by membrane distillation (Fig. 2b), and the TM (Ti) membrane, used as a porous substrate for the deposition of nanofibrous PVDF layer (Fig. 2c). It can be seen that the latter membrane has a surface structure typical of track-etched membranes [42]. The deposition of a titanium layer  $40 \pm 4$  nm thick does not change significantly the pore diameter on its surface.

FTIR spectroscopy and XRD analysis were employed to determine the chemical structure of the deposited nanofibrous layer. It is known that PVDF is

**Fig. 2.** SEM micrographs of membrane sample surfaces: (a) TM (Ti) + PVDF (10); (b) PVDF, Merck; and (c) TM (Ti).

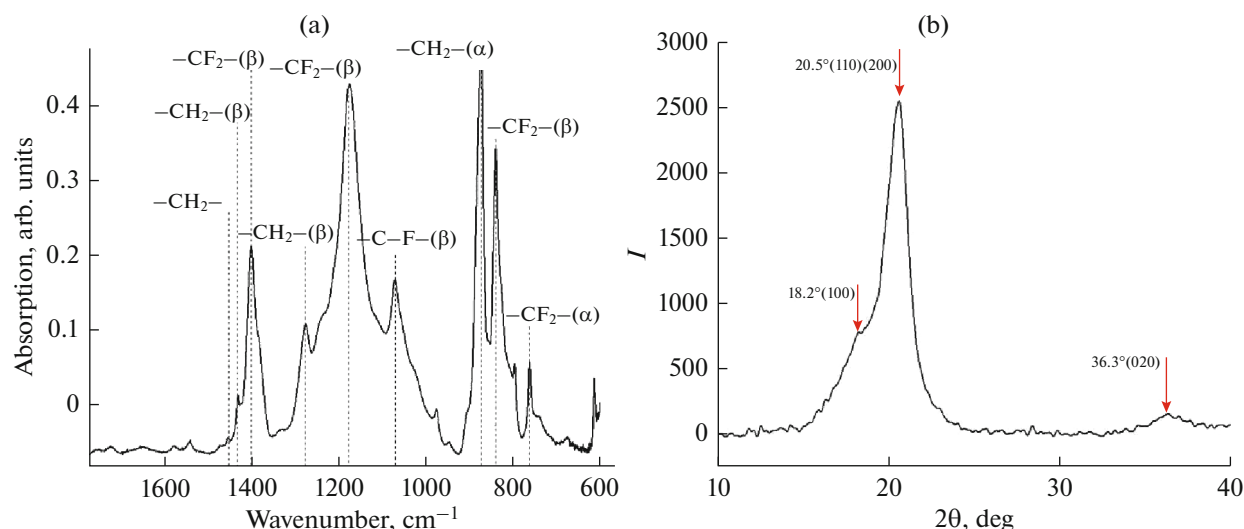


Fig. 3. (a) FTIR spectrum and (b) X-ray diffraction pattern of a nanofibrous PVDF layer on the surface of a TM (Ti) membrane.

a semicrystalline material containing four possible  $\alpha$ -,  $\beta$ -,  $\gamma$ -, and  $\delta$ -phases having different conformations of macromolecular chains [43–46]. The C–F bonds are polar, and the largest dipole moment is achieved when all polymer dipoles are oriented in the same direction, as they are in the  $\beta$ -phase of PVDF. The dipole moments of  $\alpha$ -crystallites are oriented in opposite directions, thereby leading to zero total polarization. FTIR spectroscopic examinations performed with the use of a Smart iTX attachment were employed to identify the phases of the nanofibrous PVDF layer deposited onto the surface of the TM (Ti) membrane; the spectrum of the layer is presented in Fig. 3a. It is seen that the spectrum contains the following absorption bands: an absorption band at  $1430\text{ cm}^{-1}$  corresponding to the wagging vibrations of  $\text{CH}_2$  groups, a band at  $1400\text{ cm}^{-1}$  attributed to the asymmetric stretching vibrations of  $\text{CF}_2$  groups, a band at  $1273\text{ cm}^{-1}$  assigned to the wagging vibrations of  $\text{CH}_2$  groups, a band at  $1171\text{ cm}^{-1}$  due to the symmetric stretching vibrations of  $\text{CF}_2$  groups, and a band at  $839\text{ cm}^{-1}$  attributed to the stretching vibrations  $\text{CF}_2$  groups. All these absorption bands correspond to the  $\beta$ -phase of PVDF. The spectrum also contains an absorption band at  $874\text{ cm}^{-1}$  assigned to the pendular vibrations of  $\text{CH}_2$  groups and a band at  $761\text{ cm}^{-1}$  characteristic of the skeletal vibrations of  $\text{CF}_2$  groups. The two last bands correspond to the  $\alpha$ -phase of PVDF.

Thus, we can note the prevailing intensity of the peaks assigned to the  $\beta$ -phase, and the low intensity of the peaks characteristic of the  $\alpha$ -phase. Fraction  $F_\beta$  of the  $\beta$ -phase can be calculated using the following equation [47]:

$$F_\beta = \frac{A_\beta}{1.3A_\alpha + A_\beta}, \quad (2)$$

where  $A_\alpha$  is the absorption at  $761\text{ cm}^{-1}$  and  $A_\beta$  is the absorption at  $840\text{ cm}^{-1}$ , with the determination accuracy of the absorptions being equal to 0.1%. The calculations carried out by Eq. (2) have shown that the fraction of the  $\beta$ -phase in the nanofibrous PVDF layer is 74.2%. The analysis of the IR absorption spectrum allows us to conclude that the fraction of the  $\beta$ -phase in the electrospun PVDF sample is slightly higher than that in the sample prepared by casting from a solution (64.4%) [48].

The XRD analysis has shown the presence of both  $\beta$ - and  $\alpha$ -phases in the nanofibrous PVDF layer (Fig. 3b). For example, the peak at  $2\theta = 18.2^\circ$  (100) is due to the presence of the  $\alpha$ -phase. The broad peak in the region of  $20.6^\circ$  corresponds to superimposed diffraction maxima due to the (110) and (200) planes of the  $\beta$ -phase [47]. The peak at  $2\theta = 36.3^\circ$  also belongs to the  $\beta$ -phase, namely, to the (020) crystallographic plane [48]. The ratio between the integral intensities observed in the X-ray diffraction patterns confirms the fact that the  $\beta$ -phase prevails in the nanofibrous PVDF layer on the surface of the TM (Ti) membrane. The significant content of the  $\beta$ -phase with a high dipole moment in the nanofibrous PVDF layer leads us to conclude that, in this case, the adhesion of this layer to the titanium surface increases mainly due to the ion–dipole interaction.

Studying the surface properties of the hybrid membranes has shown that the deposition of a nanofibrous PVDF layer by the electrospinning method leads to significant hydrophobization of the TM (Ti) membrane surface (Fig. 4). For example, while the surface of a track-etched PET membrane after applying a titanium layer has water contact angle  $\Theta_w$  equal to  $39.9 \pm 3.5^\circ$ , the hybrid TM (Ti) + PVDF (V) membranes have an average contact angle of  $143.3 \pm 1.3^\circ$  (Table 1); i.e., the membranes of this type are highly

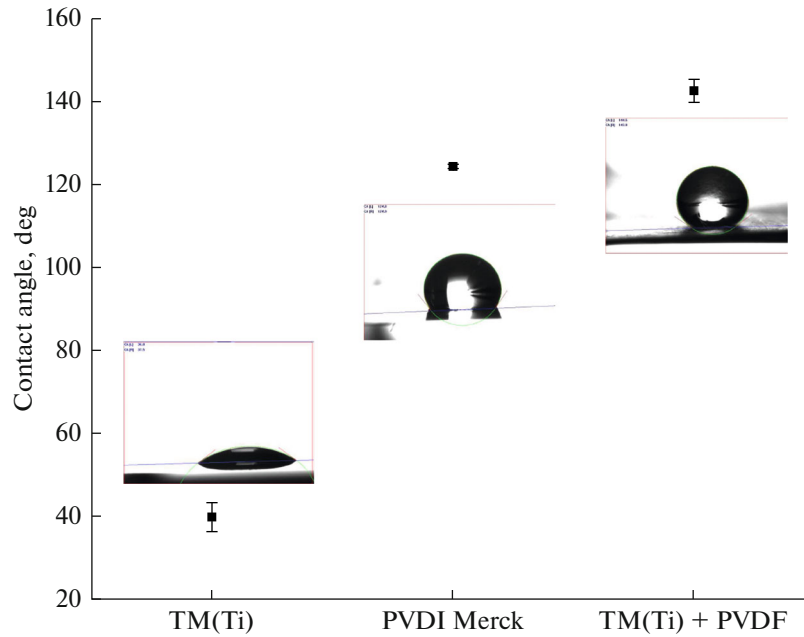


Fig. 4. Water contact angles at the surfaces of membrane samples: TM (Ti), PVDF Merck, and TM (Ti) + PVDF (10).

hydrophobic. The commercial PVDF membrane (Durapore, Merck) has a slightly lower value of  $\Theta_w$ , equal to  $124.3 \pm 0.5^\circ$ . The difference between the surface wettabilities of the studied membranes is most likely due to the higher roughness of the deposited nanofibrous layer, which has hydrophobic properties. It is known that the development of polymer roughness or the presence of deep pores on its hydrophobic surface leads to an increase in the contact angle [49, 50]. Apparently, the surface microstructure of the nanofibrous PVDF layer is organized in such a way that it provides a higher contact angle than that of the PVDF microfiltration membrane (PVDF, Merck).

Thus, the application of a nanofibrous PVDF layer by electrospinning onto a TM (Ti) membrane surface leads to the formation of hybrid membranes consisting of three layers. Two of them form a composite of a track-etched PET membrane and a layer of deposited titanium. The water contact angle of the unmodified surface of the track-etched membrane is  $72.0 \pm 1^\circ$ . The third layer is highly hydrophobic. Its average contact angle is  $143.3 \pm 1.3^\circ$ .

A water contact angle at a surface is the key parameter indicating whether a membrane is more hydrophobic than another one. However, when membranes are used for water desalination by membrane distillation, in addition to  $\Theta_w$ , an important parameter is  $LEP_w$  (liquid pressure at the membrane inlet), which is the minimum pressure required for a liquid (in this case water) to penetrate the pores of a membrane. To prevent pores from wetting, the value of  $LEP_w$  must be as high as possible. The  $LEP_w$  value for hydrophobic

membranes can be calculated by the Young–Laplace equation [51]:

$$LEP_w = \frac{-2B\gamma_L \cos\Theta_w}{r_{\max}}, \quad (3)$$

where  $B$  is a geometric factor determined by the pore structure of a membrane (in the case of cylindrical pores,  $B = 1$ ),  $\gamma_L$  is the water surface tension measured in N/m,  $r_{\max}$  is the maximum pore size of the membrane, and  $\Theta_w$  is the water contact angle at the membrane surface. According to Eq. (3), the value of  $LEP_w$  depends on the pore size and the hydrophobicity of a membrane. Hence, to reach a high value of  $LEP_w$ , membrane materials must be highly hydrophobic and, therefore, have a low surface energy and small pore sizes. Note that the choice of membranes with small pore sizes may decrease the productivity of the membrane distillation process due to their low permeability. In other words, to achieve high process productivity, the used membranes must have a high permeability and a high  $LEP_w$  value. However, geometric factor  $B$  cannot be determined for nanofibrous layers of hybrid membranes having pores of arbitrary configuration. Therefore, the value of  $LEP_w$  was determined according to the method [40] described in the Experimental section.

The values of  $LEP_w$  for hybrid membranes formed by depositing nanofibrous PVDF layers of different densities onto the surface of the TM (Ti) membrane are given in Table 1. It follows from the presented data that, in comparison with the commercial PVDF membrane (Durapore, Merck), for which the value of

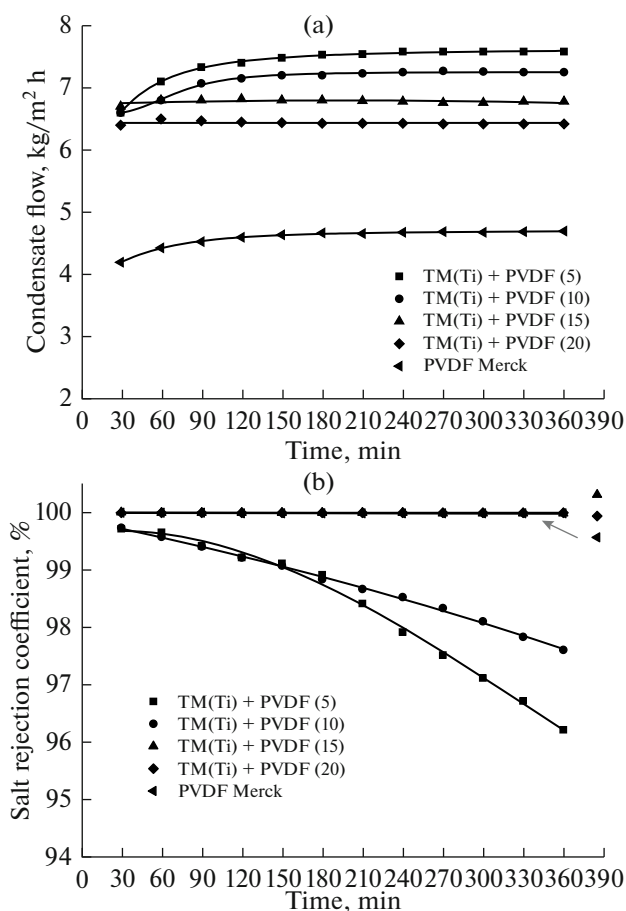


**Fig. 5.** Time variations in (a) condensate flows and (b) salt rejection coefficients during the MD process for TM (Ti) + PVDF (V) membranes with different densities of the deposited nanofibrous layer and a PVDF membrane, Merck.

$LEP_w$  is  $120 \pm 2$  kPa, the hybrid membranes show a decrease in  $LEP_w$  from  $27 \pm 1$  to  $25 \pm 1$  kPa. This means that the deposited nanofibrous PVDF layer does not have a sufficient resistance to wetting; i.e., hybrid membranes require lower pressure to force water penetration into the pores. The absence of changes in the  $LEP_w$  with variations in the density of the nanofibrous layer deposited onto the surface of the TM (Ti) membrane indicates that the hybrid membranes have identical average pore diameters and structures of the developed pore space, since the contact angles of their surfaces are almost equal. The comparison of our experimental data on the  $LEP_w$  value with the literature data has shown that the elaborated membranes are actually not inferior to the nanofibrous PVDF membranes used for water desalination by membrane distillation [24, 52]. However, in order to increase the  $LEP_w$  values of our hybrid membranes, it is apparently necessary to increase the density of the deposited nanofibrous PVDF layer by increasing either the viscosity of the working solution

or the time of the deposition process. For example, it has been shown [40] that, as the time of PVDF electrospinning is increased from 1 to 6 h,  $LEP_w$  rises from 62 to 110 kPa.

The method of air gap membrane distillation was used to determine the efficiency of aqueous sodium chloride solution separation with the studied membranes. Figure 5a shows the data on time variations in the membrane productivity. It can be seen that, during operation of the TM (Ti) + PVDF (5) and TM (Ti) + PVDF (10) membranes, the condensate flow increases to a certain maximum value at the initial stage. In this case, a hybrid membrane with the density of the deposited PVDF layer equal to  $6.9 \text{ g/m}^2$  shows a higher maximum value of the condensate flow equal to  $7.58 \pm 0.15 \text{ kg/m}^2 \text{ h}$ . As the density of the PVDF layer deposited onto the surface of the TM (Ti) membrane increases, the maximum condensate flow decreases. For example, the maximum condensate flow through a membrane with a deposited PVDF layer density of  $13.8 \text{ g/m}^2$  is equal to  $7.27 \pm 0.15 \text{ kg/m}^2 \text{ h}$ . Among the studied membranes, the highest and lowest gas permeabilities are inherent in the membranes with deposited PVDF layer densities of  $6.9$  and  $13.8 \text{ g/m}^2$ , respectively. This allows us to conclude that the efficiency of membranes in the process of membrane distillation is, primarily, governed by their gas permeability, i.e., porosity. Two hours after the onset of the tests, when the curves have reached the maximum value, the TM (Ti) + PVDF (5) and TM (Ti) + PVDF (10) membranes have shown an identical tendency to maintaining the condensate flow in the course of time. On the contrary, for the TM (Ti) + PVDF (15) and TM (Ti) + PVDF (20) membranes, the curves for the time variations in the condensate flow reach a maximum value over the first 30 min after the onset of the tests. In this case, the maximum condensate flow also depends on the density of the deposited PVDF layer, i.e., the lowest flow is observed for the TM (Ti) + PVDF (20) membrane with the density of the deposited PVDF layer equal to  $27.6 \text{ g/m}^2$ . A slightly higher value of the maximum condensate flow is inherent in the TM (Ti) + PVDF (15) membrane with a deposited PVDF layer density of  $20.7 \text{ g/m}^2$  (Table 2). This fact should be taken into account when choosing the duration of the nanofibrous PVDF layer deposition on the surface of a TM (Ti) membrane.

The comparison of the experimental data on the productivity of the hybrid membranes with that of the commercial PVDF membrane (Durapore, Merck), which has a pore size of  $0.45 \mu\text{m}$  and is used for desalinating water by membrane distillation, has shown that, when the process is carried out in a similar regime, the latter membrane is significantly inferior to the membranes that we have developed (Fig. 5a). Despite the slightly higher gas permeability compared to the hybrid membranes, the maximum condensate flow is

**Table 2.** Comparison of productivities and separation selectivities of membranes in the process of membrane distillation

Parameters	PVDF, Merck	Hybrid membranes			
		TM (Ti) + PVDF (5)	TM (Ti) + PVDF (10)	TM (Ti) + PVDF (15)	TM (Ti) + PVDF (20)
Maximum condensate flow, kg/m <sup>2</sup> h	4.68 ± 0.10	7.58 ± 0.15	7.27 ± 0.15	6.78 ± 0.12	6.45 ± 0.12
* Specific electrical conductivity of condensate, μS/cm	6.8 ± 0.5	1968 ± 10	1642 ± 10	5.3 ± 0.4	5.6 ± 0.5
* Salt concentration in condensate, mg/L	7.95 ± 0.05	934.6 ± 5.4	638.6 ± 3.2	7.96 ± 0.06	5.34 ± 0.05
* Salt rejection coefficient, %	99.97	96.47	97.59	99.97	99.98

\* After carrying out the process for 6 h.

1.5 times lower than the average maximum flow through the TM (Ti) + PVDF (V) membranes. Thus, the hybrid membranes, which consist of a hydrophilic substrate represented by a PET TM with a deposited titanium layer and a highly hydrophobic nanofibrous PVDF layer, have shown higher condensate flow values than the commercial PVDF membrane, because they provide a shorter path for vapor passing through the hydrophobic layer due to its smaller thickness and more developed pore structure. The other part of the membranes, which has the hydrophilic nature, exhibits a lower resistance to the mass transfer. It is the combination of a thin highly hydrophobic nanofibrous layer, which has a developed pore structure, with a hydrophilic microporous substrate in the hybrid membranes that leads to an increase in the productivity of the membrane distillation process in the course of desalinating an aqueous sodium chloride solution.

It should be noted that, in [23], when studying the process of membrane distillation using composite membranes consisting of a track-etched PET membrane with a pore diameter of 0.25 μm and coatings deposited from an active gaseous phase obtained by electron-beam dispersion of PTFE, we observed a tendency to a decrease in the condensate flow with time. After reaching the maximum values, the condensate flows began to gradually decrease until the end of the experiment. For example, a decrease in the condensate flow by 0.6% was recorded in 6 h for a composite membrane coated with a PTFE layer having a thickness of 100 nm. For a membrane with a deposited PTFE layer 300 nm thick, this value was 1.5%, and, for a membrane with a coating 500 nm thick, it was 1.7%. A similar time dependence of the condensate flow was observed for the initial track-etched membranes made of PET and PP. For them, the condensate flow also increased to a certain maximum value at an initial stage; then, the flow began to gradually decrease. We have assumed that the main reason for the decrease in the productivity of the composite and original track-etched membranes is, most likely, the design of a

membrane separation module. The analysis of the experimental data led us to conclude that the use of a porous Caprolon sheet with a low thermal conductivity coefficient (0.35 W/m K) in [23] as a substrate for membranes located in MDMs apparently led to the condensation of water vapor in membrane pores. This hindered the mass transfer at a certain stage of the MD process and led to a decrease in the productivity with time. In this work, when studying the membrane distillation process, we used a porous brass sheet as a substrate for membranes located in an MDM. The thermal conductivity coefficient of the brass sheet was significantly higher, i.e., 85.5 W/m K. As a result of replacing the substrate, no significant overcooling of the membranes in the MDM was observed and, probably, water vapor was not condensed in the pores.

Table 2 presents the comparison between the separation selectivities of the hybrid membranes during desalination of an aqueous 26.5 g/L sodium chloride solution (specific electrical conductivity of 49.70 mS/cm) by membrane distillation. In addition, Table 2 shows the data on the separation selectivity of the commercial PVDF membrane (Durapore, Merck) with a pore diameter of 0.45 μm. It can be seen that the studied TM (Ti) + PVDF (15) and TM (Ti) + PVDF (20) hybrid membranes ensure a high separation selectivity comparable with the selectivity of the commercial PVDF membrane. As a result of the membrane distillation process, the salt content in water is reduced, on average, by more than 4000 times. The salt rejection coefficient in the studied process is 99.97–99.98% throughout the process (Fig. 5b). For the TM (Ti) + PVDF (5) and TM (Ti) + PVDF (10) membranes, a decrease in the salt rejection coefficient is observed during membrane distillation (Fig. 5b). This finding may, apparently, be explained by possible wetting of the surface of the nanofibrous layer of the membranes due to the low deposition density, which facilitates the penetration of the salt into the condensate. For comparison, let us note that the initial PET TM possessing hydrophilic properties has low separa-

tion selectivity during membrane distillation. As has been shown in [23], the coefficient of salt rejection during the separation of an aqueous 15.0 g/L sodium chloride solution is equal to 53.45%, while the salt content in the condensate at the end of the process is 6.98 g/L.

Thus, the problem of producing highly efficient hybrid membranes that we have developed for the purpose of their use for water desalination is associated with determining a sufficient but necessary density of the nanofibrous PVDF layer deposited onto the surface of the TM (Ti) membrane. On the one hand, this problem is associated with a sufficient density of this layer, which would lead to a noticeable increase in the contact angle of the initial membrane (i.e., the manufactured hybrid membranes should be highly hydrophobic but should not cause a noticeable decrease in the productivity of the membrane distillation process). The performed experiments have shown that, to attain this purpose, it is sufficient to deposit a layer with a density of 6.9 g/m<sup>2</sup>. In this case, the surface of the nanofibrous layer will have highly hydrophobic properties. On the other hand, it is necessary to choose the density of the deposited nanofibrous layer that would ensure a high salt rejection coefficient during membrane distillation. Selection of the optimum density of the deposited PVDF layer ranging from 20.7 ± 0.2 to 27.6 ± 0.2 g/m<sup>2</sup> ensures the formation of hybrid membranes that have a highly hydrophobic surface, sufficient productivity, and a high salt rejection coefficient. This makes it possible to use them for water desalination by membrane distillation.

## CONCLUSIONS

The following conclusions can be inferred from the obtained results. The deposition of nanofibrous PVDF coatings onto the surface of a TM (Ti) membrane by electrospinning leads to the formation of hybrid membranes consisting of three layers. Two of them form a composite of a track-etched PET membrane and a layer of deposited titanium. The water contact angle at the unmodified surface of the track-etched membrane is 72.0 ± 1°. The third layer composed of PVDF nanofibers has highly hydrophobic properties. The contact angle of this layer slightly varies depending on the deposition density and is, on average, equal to 143.3 ± 1.3°.

The SEM morphological studies of the electrospun PVDF layer have shown that it consists of randomly arranged nanofibers, i.e., it has a microstructure typical of nonwoven materials. The nanofibers forming the porous system of this layer have a wide scatter of sizes. The studies of the molecular structure of the deposited nanofibrous layer by the methods of FTIR spectroscopy and XRD analysis have shown that the β-phase prevails in its structure and amounts to 74.2% of the layer. This is slightly higher than that in the sam-

ple prepared by casting from a solution, for which the fraction of the β-phase is 64.4%.

The developed hybrid membranes provide a high separation selectivity of desalinating an aqueous sodium chloride solution by membrane distillation. The salt rejection coefficient in the studied regime of the membrane distillation process is 99.97–99.98%. Moreover, the membranes have shown higher condensate flow values than the commercial PVDF membrane (Durapore, Merck), because the hybrid membranes provide a shorter path for vapor to penetrate through a highly hydrophobic layer owing to its smaller thickness and more developed porous structure. The other part of the membranes, which has a hydrophilic nature, creates a weaker resistance to the mass transfer. It is the combination of a thin highly hydrophobic layer, which has a developed porous structure, with a hydrophilic microporous substrate in the composition of the hybrid membranes that leads to an increase in the productivity of membrane distillation in the process of desalinating an aqueous sodium chloride solution. The distillate obtained by the MD process meets the requirements imposed on drinking water and process water used in many industries.

Thus, the functionalization of a hydrophilic microporous TM (Ti) membrane by the deposition of a nanofibrous PVDF layer on its surface makes it possible to finely tune the chemical and physical properties of the resulting hybrid membranes, including their wettability. The formation of a highly hydrophobic layer of PVDF nanofibers leads to the creation of membranes with high selectivity of the separation of an aqueous sodium chloride solution by membrane distillation. Moreover, the combination of a thin highly hydrophobic nanofibrous layer having a developed porous structure with a hydrophilic microporous substrate in hybrid membranes leads to an increase in the productivity of the membrane distillation process employed for water desalination.

## ACKNOWLEDGMENTS

The authors are grateful to N.E. Lizunov and O.L. Orelovich for performing electron microscopic studies.

## FUNDING

This work was supported by ongoing institutional funding of the Joint Institute of Nuclear Research. No additional grants to carry out or direct this particular research were obtained.

## CONFLICT OF INTEREST

The authors of this work declare that they have no conflicts of interest.

## REFERENCES

- Curto, D., Franzitta, V., and Guercio, A., A review of the water desalination technologies, *Appl. Sci.*, 2021, vol. 11, p. 670.  
<https://doi.org/10.3390/app11020670>
- Bryk, M.T. and Nigmatullin, R.R., Membrane distillation, *Russ. Chem. Rev.*, 1994, vol. 63, pp. 1047–1062.  
<https://doi.org/10.1070/RC1994v063n12ABEH000133>
- Drioli, E., Ali, A., and Macedonio, F., Membrane distillation: Recent developments and perspectives, *Desalination*, 2015, vol. 356, pp. 56–84.  
<https://doi.org/10.1016/j.desal.2014.10.028>
- Essalhi, M. and Khayet, M., Surface segregation of fluorinated modifying macromolecule for hydrophobic/hydrophilic membrane preparation and application in air gap and direct contact membrane distillation, *J. Membr. Sci.*, 2012, vols. 417–418, pp. 163–173.
- Khalifa, A., Lawal, D., Antar, M., and Khayet, M., Experimental and theoretical investigation on water desalination using air gap membrane distillation, *Desalination*, 2015, vol. 376, pp. 94–108.  
<https://doi.org/10.1016/j.desal.2015.08.016>
- Woo, Yu.Ch., Tijing, L.D., Park, M.J., Yao, M., Choi, J.-S., Lee, S., Kim, S.-H., An, K.-J., and Shon, H.K., Electrospun dual-layer nonwoven membrane for desalination by air gap membrane distillation, *Desalination*, 2017, vol. 404, pp. 187–198.  
<https://doi.org/10.1016/j.desal.2015.09.009>
- Ulbricht, M., Advanced functional polymer membranes, *Polymer*, 2006, vol. 47, pp. 2217–2262.  
<https://doi.org/10.1016/j.polymer.2006.01.084>
- Blasco, E., Sims, M.B., Goldmann, A.S., Sumerlin, B.S., and Barner-Kowollik, C., 50th anniversary perspective: Polymer functionalization, *Macromolecules*, 2017, vol. 50, pp. 5215–5252.  
<https://doi.org/10.1021/acs.macromol.7b00465>
- Makvandi, P., Iftekhhar, S., Pizzetti, F., Zarepour, A., Zare, E.N., Ashrafzadeh, M., Agarwa, T., Padil, V.V.T., Mohammadinejad, R., Sillanpaa, M., Maiti, T.K., Perale, G., Zarrabi, A., and Rossi, F., Functionalization of polymers and nanomaterials for water treatment, food packaging, textile and biomedical applications: A review, *Environ. Chem. Lett.*, 2021, vol. 19, pp. 583–611.  
<https://doi.org/10.1007/s10311-020-01089-4>
- Abegunde, O.O., Akinlabi, E.T., Oladijo, O.Ph., Akinlabi, S., and Ude, A.U., Overview of thin film deposition techniques, *AIMS Mater. Sci.*, 2019, vol. 6, pp. 174–199.  
<https://doi.org/10.3934/matensci.2019.2.174>
- Liu, F., Wang, L., Li, D., Liu, Q., and Deng, B., A review: The effect of the microporous support during interfacial polymerization on the morphology and performances of a thin film composite membrane for liquid purification, *RCS Adv.*, 2019, vol. 9, pp. 35417–35428.  
<https://doi.org/10.1039/c9ra07114h>
- Anis, Sh.F., Hashaikeh, R., and Hilal, N., Functional materials in desalination: A review, *Desalination*, 2019, vol. 468, p. 114077.  
<https://doi.org/10.1016/j.desal.2019.114077>
- Assad, M. El Haj, Bani-Hanib, E., Al-Sawafta, I., Issa, S., Hmida, A., Gupta, M., Atiqure, R.S.M., and Hidouri, K., Applications of nanotechnology in membrane distillation: A review study, *Desalin. Water Treat.*, 2020, vol. 192, pp. 61–77.  
<https://doi.org/10.5004/dwt.2020.25821>
- Farahbakhsh, J., Vatanpour, V., Khoshnam, M., and Zargar, M., Recent advancements in the application of new monomers and membrane modification techniques for the fabrication of thin film composite membranes: A review, *React. Funct. Polym.*, 2021, vol. 166, p. 105015.  
<https://doi.org/10.1016/j.reactfunctpolym.2021.105015>
- Kravets, L.I., Altynov, V.A., Yarmolenko, M.A., Gainutdinov, R.V., Satulu, V., Mitu, B., and Dinescu, G., Deposition on the track-etched membranes surface of hydrophobic polymer coatings from the active gas phase, *Membr. Membr. Technol.*, 2022, vol. 4, no. 2, pp. 133–143.  
<https://doi.org/10.1134/S251775162202007X>
- Fan, W., Qian, J., Bai, F., Li, Y., Wang, C., and Zhao, Q.-Z., A facile method to fabricate superamphiphobic polytetrafluoroethylene surface by femtosecond laser pulses, *Chem. Phys. Lett.*, 2016, vol. 644, pp. 261–266.  
<https://doi.org/10.1016/j.cplett.2015.12.010>
- Yong, J., Chen, F., Yang, Q., Jiang, Z., and Hou, X., A review of femtosecond-laser-induced underwater superoleophobic surfaces, *Adv. Mater. Interfaces*, 2018, vol. 5, p. 1701370.  
<https://doi.org/10.1002/admi.201701370>
- Satulu, V., Mitu, B., Pandeale, A.M., Voicu, S.I., Kravets, L., and Dinescu, G., Composite polyethylene terephthalate track membranes with thin teflon-like layers: Preparation and surface properties, *Appl. Surf. Sci.*, 2019, vol. 476, pp. 452–459.  
<https://doi.org/10.1016/j.apsusc.2019.01.109>
- Ju, Y., Ai, L., Qi, X., Li, J., and Song, W., Review on hydrophobic thin films prepared using magnetron sputtering deposition, *Materials*, 2023, vol. 16, p. 3764.  
<https://doi.org/10.3390/ma16103764>
- Michels, A.F., Soave, P.A., Nardi, J., Jardim, P.L.G., Teixeira, S.R., Weibel, D.E., and Horowitz, F., Adjustable, (super)hydrophobicity by e-beam deposition of nanostructured PTFE on textured silicon surfaces, *J. Mater. Sci.*, 2016, vol. 51, pp. 1316–1323.  
<https://doi.org/10.1007/s10853-015-9449-3>
- Grytsenko, K., Ksianzou, V., Kolomzarov, Y., Lytvyn, P., Dietzel, B., and Schrader, S., Fluoropolymer film formation by electron activated vacuum deposition, *Surfaces*, 2021, vol. 4, pp. 66–80.  
<https://doi.org/10.3390/surfaces4010009>
- Kravets, L.I., Yarmolenko, M.A., Rogachev, A.A., Gainutdinov, R.V., Gilman, A.B., Altynov, V.A., and Lizunov, N.E., Formation of superhydrophobic coatings on the track-etched membrane surface by the method of electron-beam dispersion of polymers in vacuum, *Inorg. Mater. App. Res.*, 2020, vol. 11, no. 2, pp. 476–487.  
<https://doi.org/10.1134/S2075113320020203>
- Kravets, L.I., Yarmolenko, M.A., Rogachev, A.V., Gainutdinov, R.V., Altynov, V.A., and Lizunov, N.E., Formation of hydrophobic and superhydrophobic coatings on track-etched membrane surfaces to create composite membranes for water desalination, *Colloid J.*,

- 2022, vol. 84, no. 4, pp. 427–444.  
<https://doi.org/10.1134/S1061933X22040081>
24. Khayet, M., Garcia-Payo, M.C., Garcia-Fernandez, L., and Contreras-Martinez, J., Dual-layered electrospun nanofibrous membranes for membrane distillation, *Desalination*, 2018, vol. 426, pp. 174–184.  
<https://doi.org/10.1016/j.desal.2017.10.036>
  25. Huang, Y., Huang, Q.-L., Liu, H., Zhang, Ch.-X., You, Y.-W., Li, N.-N., and Xiao, Ch.-F., Preparation, characterization, and applications of electrospun ultra-fine fibrous PTFE porous membranes, *J. Membr. Sci.*, vol. 523, pp. 317–326.  
<https://doi.org/10.1016/j.memsci.2016.10.019>
  26. Tijing, L.D., Choi, J.S., Lee, S., Kim, S.H., and Shon, H.K., Recent progress of membrane distillation using electrospun nanofibrous membrane, *J. Membr. Sci.*, 2014, vol. 453, pp. 435–462.  
<https://doi.org/10.1016/j.memsci.2013.11.022>
  27. Subrahmanya, T.M., Arshad, A.B., Lin, P.T., Widakdo, J., Makari, H.K., Austria, H.F.M., Hu, Ch.-Ch., Lai, J.Y., and Hung, W.-S., A review of recent progress in polymeric electrospun nanofiber membranes in addressing safe water global issues, *RSC Adv.*, 2021, vol. 11, pp. 9638–9663.  
<https://doi.org/10.1039/d1ra00060h>
  28. Nayl, A.A., Abd-Elhamid, A.I., Awwad, N.S., Abdelgawad, M.A., Wu, J., Mo, X., Gomha, S.M., Aly, A.A., and Brase, S., Review of the recent advances in electrospun nanofibers applications in water purification, *Polymers*, 2022, vol. 14, p. 1594.  
<https://doi.org/10.3390/polym14081594>
  29. Khatri, M., Francis, L., and Hilal, N., Modified electrospun membranes using different nanomaterials for membrane distillation, *Membranes*, 2023, vol. 13, p. 338.  
<https://doi.org/10.3390/membranes13030338>
  30. Filatov, Yu.N., *Elektroformovanie voloknistykh materialov (EfV-Protess)* (Electroforming of Fibrous Materials (EFV-Process)), Moscow, 2001.
  31. Kolobkov, A.S., Electroforming of synthetic fibres and their applications (overview), *Nanoindustriya*, 2022, vol. 15, no. 2, pp. 118–127.  
<https://doi.org/10.22184/1993-8578.2022.15.2.118.127>
  32. Vinogradov, I.I., Petrik, L., Serpionov, G.V., and Nechaev, A.N., Composite membrane based on track-etched membrane and chitosan nanoscaffold, *Membr. Membr. Technol.*, 2021, vol. 3, no. 6, pp. 400–410.  
<https://doi.org/10.1134/S2517751621060093>
  33. Vinogradov, I.I., Andreev, E.V., Yushin, N.S., Sokhatskii, A.S., Altynov, V.A., Gustova, M.V., Vershinina, T.N., Zinkovskaya, I., Nechaev, A.N., and Apel, P.Yu., A hybrid membrane for the simultaneous selective sorption of cesium in the ionic and colloid forms, *Theor. Found. Chem. Eng.*, 2023, vol. 57, no. 4, pp. 549–562.  
<https://doi.org/10.1134/S0040579523040498>
  34. Perea, O., Uche, C., Bublikov, P.S., Bode-Aluko, C., Rossouw, A., Vinogradov, I.I., Nechaev, A.N., Opeolu, B., and Petrik, L., Chitosan/PEO nanofibers electrospun on metallized track-etched membranes: Fabrication and characterization, *Mater. Today Chem.*, 2021, vol. 20, p. 100416.  
<https://doi.org/10.1016/j.mtchem.2020.100416>
  35. Rossouw, A., Olejniczak, A., Olejniczak, K., Gorbeg, B., Vinogradov, I., Kristavchuk, O., Nechaev, A., Petrik, L., Perold, W., and Dmitriev, S., Ti and TiO<sub>2</sub> magnetron sputtering in roll-to-roll fabrication of hybrid membranes, *Surf. Interface*, 2022, vol. 31, p. 101975.  
<https://doi.org/10.1016/j.surfin.2022.101975>
  36. Demina, T.S., Frolova, A.A., Istomin, A.V., Kotova, S.L., Piskarev, M.S., Bardakova, K.N., Yablokov, M.Y., Altynov, V.A., Karavets, L.I., Gilman, A.B., Akopova, N.A., and Timashev, P.S., Coating of polylactide films by chitosan: Comparison of methods, *J. Appl. Polym. Sci.*, 2020, vol. 137, no. 3, p. 48267.  
<https://doi.org/10.1002/app.48287>
  37. Apel, P.Yu. and Dmitriev, S.N., Micro- and nanoporous materials produced using accelerated heavy ion beams, *Adv. Nat. Sci.: Nanosci. Nanotechnol.*, 2011, vol. 2, p. 013002.  
<https://doi.org/10.1088/2043-6262/2/1/013002>
  38. Almarzooqi, F.A., Bilad, M.R., and Arafat, H.A., Development of PVDF membranes for membrane distillation via vapour induced crystallisation, *Eur. Polym. J.*, 2016, vol. 77, pp. 164–173.  
<https://doi.org/10.1016/j.eurpolymj.2016.01.031>
  39. Huhtamäki, T., Tian, X., Korhonen, J.T., and Ras, R.H.A., Surface-wetting characterization using contact angle measurements, *Nat. Protoc.*, 2018, vol. 13, pp. 1521–1538.  
<https://doi.org/10.1038/s41596-018-0003-z>
  40. Essalhi, M. and Khayet, M., Self-sustained webs of polyvinylidene fluoride electrospun nanofibers at different electrospinning times: 1. Desalination by direct contact membrane distillation, *J. Membr. Sci.*, 2013, vol. 433, pp. 167–179.  
<https://doi.org/10.1016/j.memsci.2013.11.056>
  41. Larkin, P.J., *Infrared and Raman Spectroscopy: Principles and Spectral Interpretation*, Waltham: Elsevier, 2011.
  42. Rossouw, A., Vinogradov, I.I., Serpionov, G.V., Gorbeg, B.L., Molokanova, L.G., and Nechaev, A.N., Composite track membrane produced by roll technology of magnetron sputtering of titanium nanolayer, *Membr. Membr. Technol.*, 2022, vol. 4, no. 3, pp. 177–188.  
<https://doi.org/10.1134/S2517751622030039>
  43. Lovinger, A.J., Poly(vinylidene fluoride), in *Developments in Crystalline Polymers*, Dordrecht: Springer, 1982, pp. 195–273.  
[https://doi.org/10.1007/978-94-009-7343-5\\_5](https://doi.org/10.1007/978-94-009-7343-5_5)
  44. Liu, F., Hashim, N.A., Liu, Y., Abed, M.R.M., and Li, K., Progress in the production and modification of PVDF membranes, *J. Membr. Sci.*, 2011, vol. 375, pp. 1–27.  
<https://doi.org/10.1016/j.memsci.2011.03.014>
  45. Kang, G.-d. and Cao, Y.-m., Application and modification of poly(vinylidene fluoride) (PVDF) membranes—A review, *J. Membr. Sci.*, 2014, vol. 463, pp. 145–165.  
<https://doi.org/10.1016/j.memsci.2014.03.055>

46. Martins, P., Lopes, A.C., and Lanceros-Mendez, S., Electroactive phases of poly(vinylidene fluoride): Determination, processing and applications, *Prog. Polym. Sci.*, 2014, vol. 39, pp. 683–706.  
<https://doi.org/10.1016/j.progpolymsci.2013.07.006>
47. Kumarasinghe, H.U., Bandara, L.R.A.K., Bandara, T.M.W.J., Senadeera, G.K.R., and Thotawatthage, C.A., Fabrication of  $\beta$ -phase poly(vinylidene fluoride) piezoelectric film by electrospinning for nanogenerator preparations, *Ceylon J. Sci.*, 2021, vol. 50, pp. 357–363.  
<https://doi.org/10.4038/cjs.v50i5.7925>
48. Lei, T., Cai, X., Wang, X., Yu, L., Hu, X., Zheng, G., Lv, W., Wang, L., Wu, D., Sun, D., and Lin, L., Spectroscopic evidence for a high fraction of ferroelectric phase induced in electrospun polyvinylidene fluoride fibers, *RSC Adv.*, 2013, vol. 3, pp. 24952–24958.  
<https://doi.org/10.1039/c3ra42622j>
49. Quere, D., Wetting and roughness, *Annu. Rev. Mater. Res.*, 2008, vol. 38, pp. 71–99.  
<https://doi.org/10.1146/annurev.matsci.38.060407.132434>
50. Boinovich, L.B. and Emelyanenko, A.M., Hydrophobic materials and coatings: principles of design, properties and applications, *Usp. Khim.*, 2008, vol. 77, pp. 583–600.  
<https://doi.org/10.1070/RC2008V077N07ABEH003775>
51. Racz, G., Kerker, S., Kovacs, Z., Vatai, G., Ebrahimi, M., and Czermak, P., Theoretical and experimental approaches of liquid entry pressure determination in membrane distillation processes, *Period. Polytech., Chem. Eng.*, 2014, vol. 58, no. 2, pp. 81–91.  
<https://doi.org/10.3311/PPch.2179>
52. Liao, Y., Wang, R., Tian, M., Qiu, Ch., and Fane, A.G., Fabrication of polyvinylidene fluoride (PVDF) nanofiber membranes by electro-spinning for direct contact membrane distillation, *J. Membr. Sci.*, 2013, vols. 425–426, pp. 30–39.  
<https://doi.org/10.1016/j.memsci.2012.09.023>

**Publisher's Note.** Pleiades Publishing remains neutral with regard to jurisdictional claims in published maps and institutional affiliations. AI tools may have been used in the translation or editing of this article.